



Introduction

River discharge is one of the essential climate variables in the water cycle which regulates the climate system and indicates its changes. Even though the necessity of river discharge information for different applications related to water resources management is well known, many basins are not still gauged and, recently the gauged ones are also declining and inaccessibility of data due to different socio-economic and political reasons contributes to the global problem (Tarpanelli et al. 2013; Sneeuw et al. 2014; Hossain et al. 2014; Gleason and Hamdan 2015; Tourian et al., 2017; Gleason et al., 2018; Feng et al. 2019). It is particularly important to note that many small to medium-sized rivers (Meybeck et al. 1996; Sulistioadi et al. 2015) are also poorly monitored (Alsdorf and Lettenmaier 2003; Alsdorf et al., 2007; Huang et al. 2019) and small-scale headwater catchments including high-mountain regions of Tibetan Plateau (TP) Rivers are mostly ungauged (Huang et al. 2019).

Remote sensing technology has a great potential to fill the existing gaps of discharge estimation in natural channels by providing a promising and viable streamflow information to efficiently monitor water resources with high correlation of satellite-derived surface hydraulic parameters (e.g. effective river width, depth and velocity) and the corresponding in-situ gauged discharge. (Tang et al., 2009; Sun et al., 2010, 2012; Sulistioadi et al., 2015; Sichangi et al., 2016, 2018; Wang et al., 2019). A successful remote sensing based discharge estimation technique will always depend on the accuracy of the estimated parameters that can be directly (width, slope and stage) or indirectly (velocity and bathymetry depth) obtained from satellite sensors and the techniques related with the measurement of these multiple hydraulic variables (Bjerklie et al. 2003; Pan and Nichols 2013; Pan, et al., 2016; Sichangi et al. 2016, 2018). Therefore, the main objective of this study is to estimate the discharge of Lhasa River flowing over the complex high-mountain regions of the TP by combing remote sensing derived and empirical equation based input parameters in to a three known discharge estimation equations/models.

Materials and methods

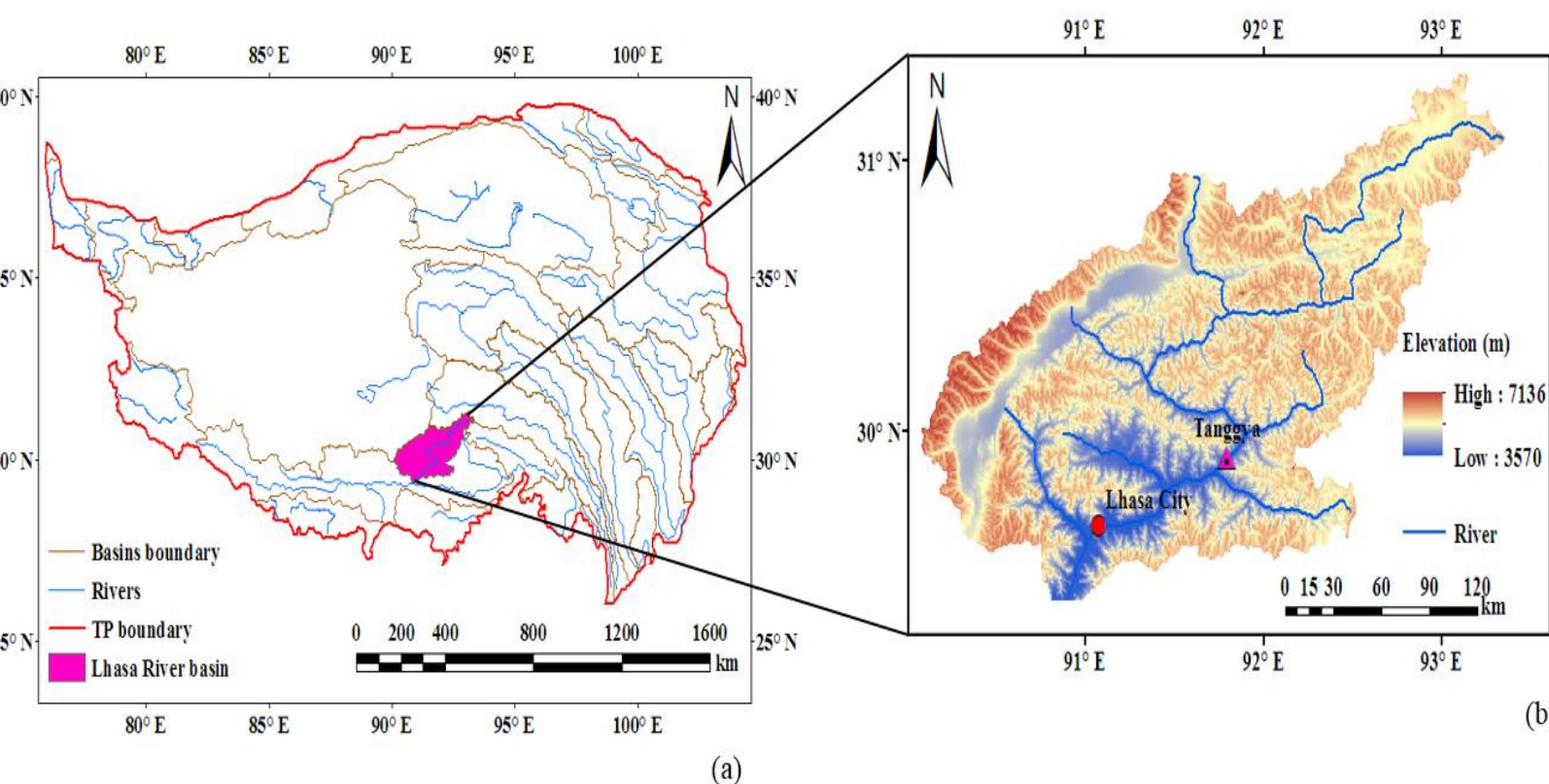


Fig. 1. Geographical location of the Tibetan Plateau region (a) & the elevation of the Lhasa River basin (LRB) based on the digital elevation model (DEM) from the Shuttle Radar Topography Mission (SRTM) (b).

The SRTM DEM was used to derive channel slope (S) & the channel roughness coefficient (n) was estimated with the help of published values & further classification of Landsat images.

To attain the aim of this study, we have extracted the water surface inundation area or effective river width (W) from high-resolution Landsat images by considering an appropriate channel reach length in a non-braided section of the Lhasa River around Tanggya gauge location. Due to lack of satellite altimetry data for water level estimation in our narrow river channel flowing over a complex high-mountain region, the mean flow depth (D) were estimated from the other satellite derived surface hydraulic parameters by using regression relations of Moody and Troutman 2002. By combining river surface hydraulic variables directly derived from remote sensing datasets (width & slope) with other variables indirectly derived from empirical equations (depth & channel roughness coefficient), we had estimated the discharge (Q) of Lhasa River by using modified Manning equation (Model 1), Bjerklie et al. (2003) equation (Model 2), and Rating curve approach (Model 3). Finally the performance of the models/equations were evaluated by using statistical metrics (RMSE, RRMSE, NSE, MBE & RE).

$$\text{Model 1: } Q = \frac{1}{n} W D^{3/2} S^{1/2} \quad \text{Model 2: } Q = 7.22 W^{1.02} D^{1.74} S^{0.35} \quad \text{Model 3: } W = a Q^b$$

where a and b are calibrated numerical constants identified in deriving the hydraulic relationship.

Results and discussion

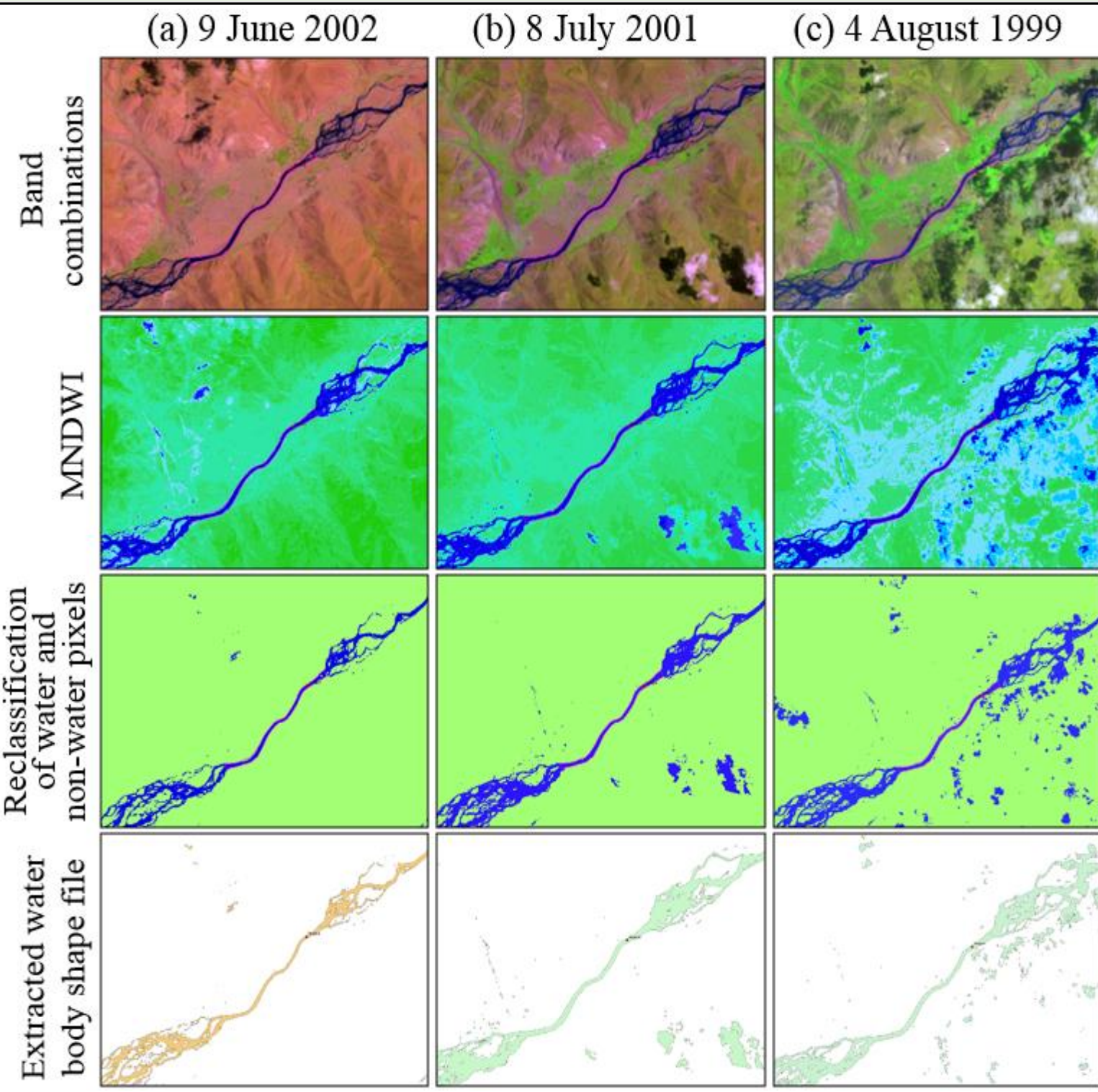


Fig. 2. An examples of Landsat image classification to estimate water surface area and/or effective width of Lhasa River during 4 August 1999 (a), 8 July 2001 (b), and 9 June 2002 (c) among 52 cloud free Landsat images used in this study: The Landsat images were further classified and combination of bands (visible and near infrared bands) with false colour were used to identify the water pixels of the river from the other non-water pixels and then the water mask has been extracted to estimate the average effective width of Lhasa River at Tanggya gauging station by using the MNDWI approach.

The effective river width (bank to bank river width) which was estimated as the ratio of water surface area to the appropriate reach length considered in this study during 4 August 1999, 8 July 2001, and 9 June 2002 were **108.4 m**, **130.0 m** and **108.6 m**, respectively.

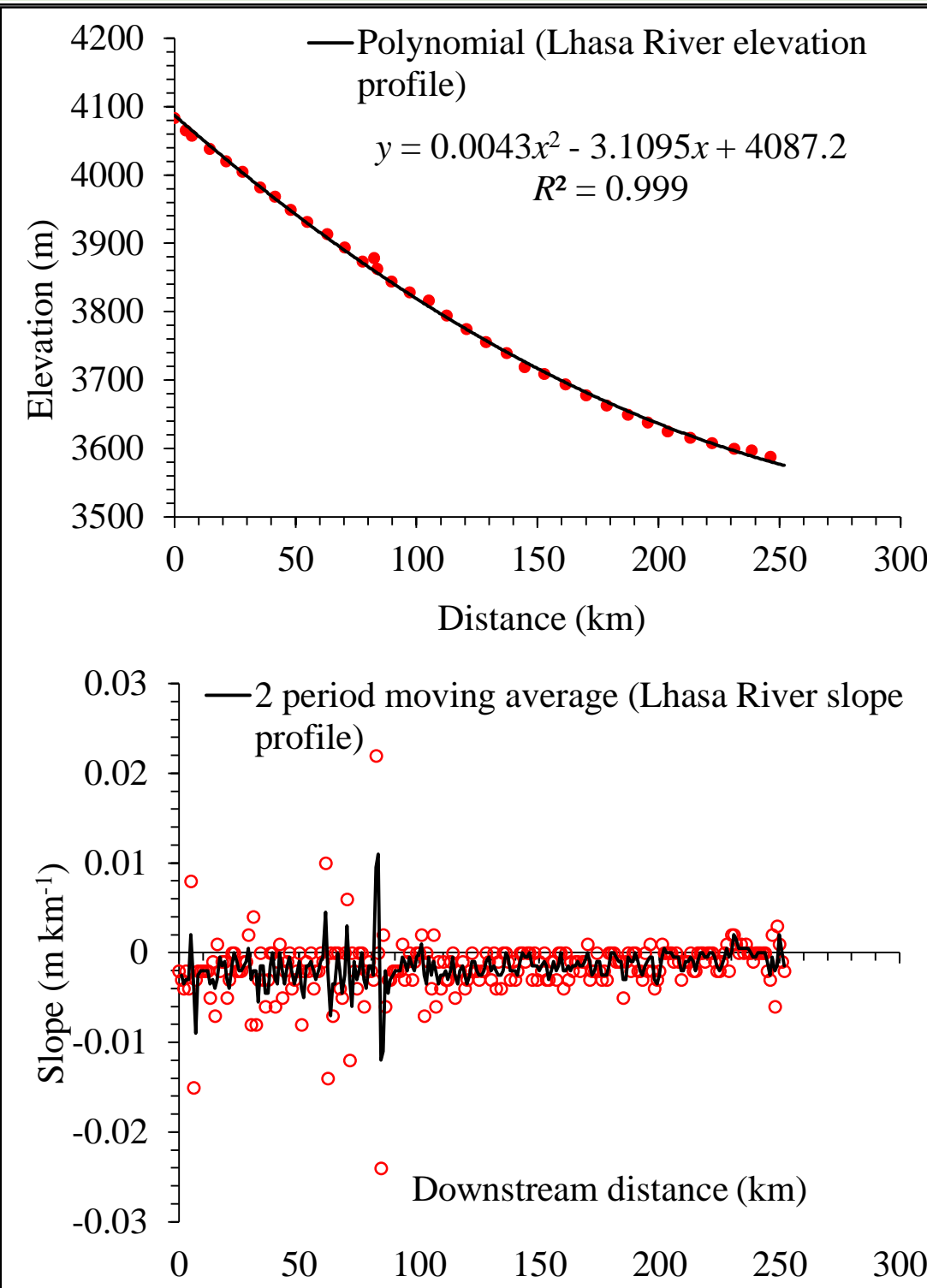


Fig. 3. We calculated the slope of the Lhasa River viably over its appropriate reach length (RL) from the SRTM DEM by extending its RL (over which discharge gauge site is located) to a sufficient distances that can accommodate the height variations so as to minimize the errors introduced in slope estimations. The altitude of river's centreline was derived from the SRTM DEM. For 252 km course of Lhasa River considered from upstream of the Zhikong dam site to its mouth at the junction of Yarlung Zangpo River, the resultant mean height error was **1.98 m km⁻¹** and its standard deviation was **3.67 m km⁻¹**. The average slope for this mentioned section of the channel was **0.002 m m⁻¹**. By considering the LRB's topography the change in slope is estimated to be cm over km.

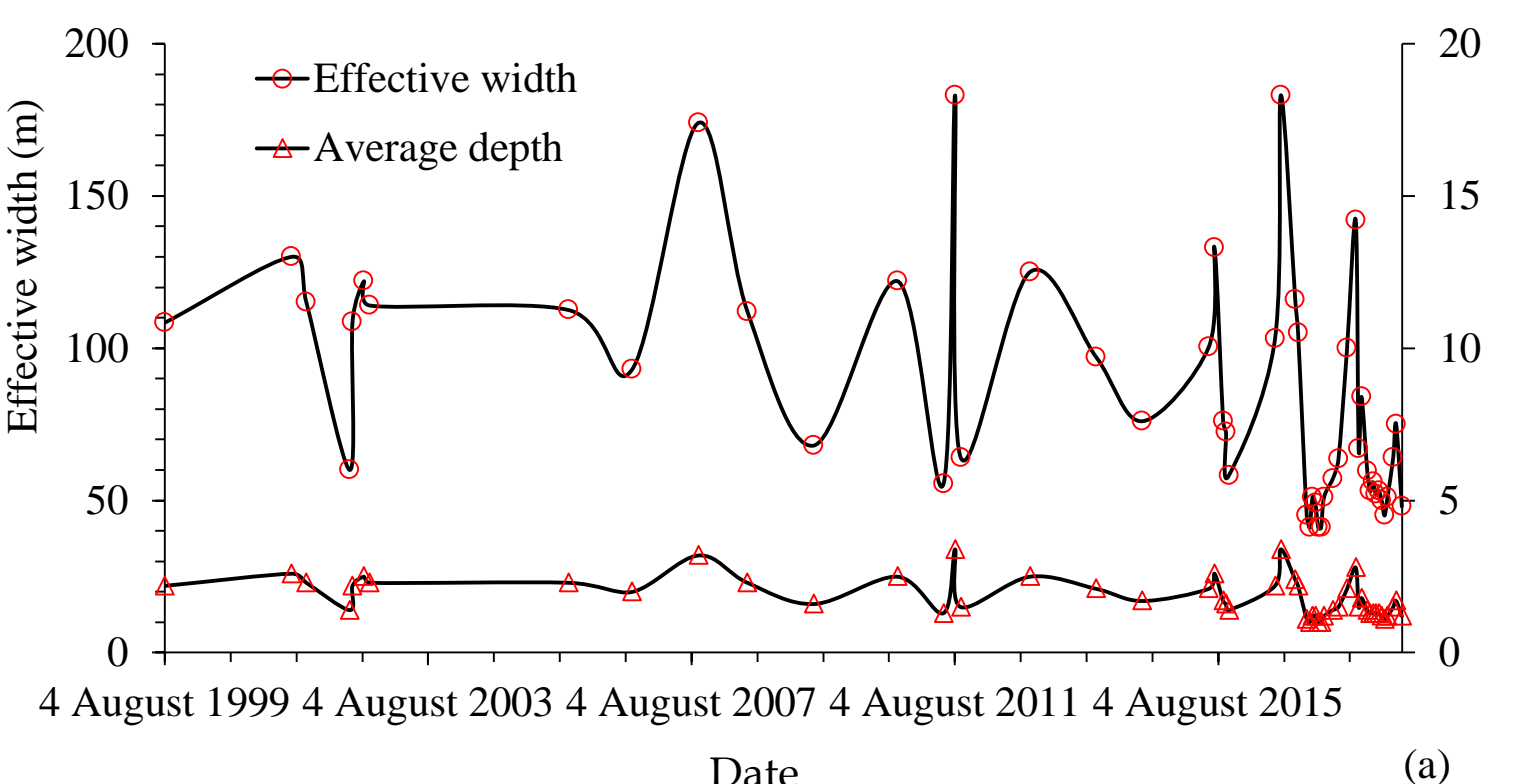


Fig. 4. The time series of effective width and average depth of Lhasa River derived from 52 clouds free Landsat images during 1999–2018. The highest effective width was estimated to be 183 m which is attributed from a historical peak discharge of $1,395 \text{ m}^3 \text{ s}^{-1}$ recorded on 5 August 2011. Historical peak discharge events are occurred during the summer monsoon season particularly on 11 September 2007 ($1,200 \text{ m}^3 \text{ s}^{-1}$), 17 July 2016 ($1,344 \text{ m}^3 \text{ s}^{-1}$), and 5 August 2011 ($1,395 \text{ m}^3 \text{ s}^{-1}$) resulting in higher river width and depth values. Both average depth and effective width shows a strong power relationship with observed discharge.

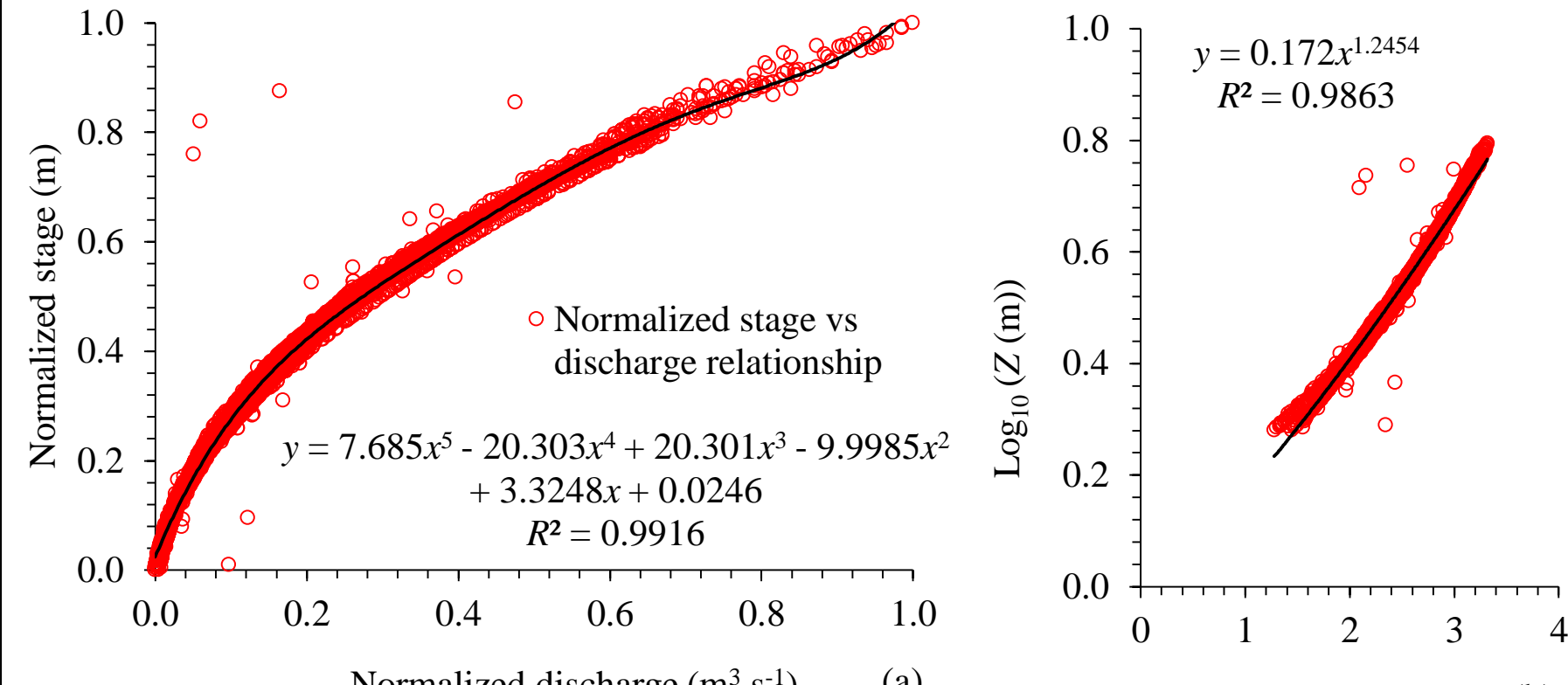
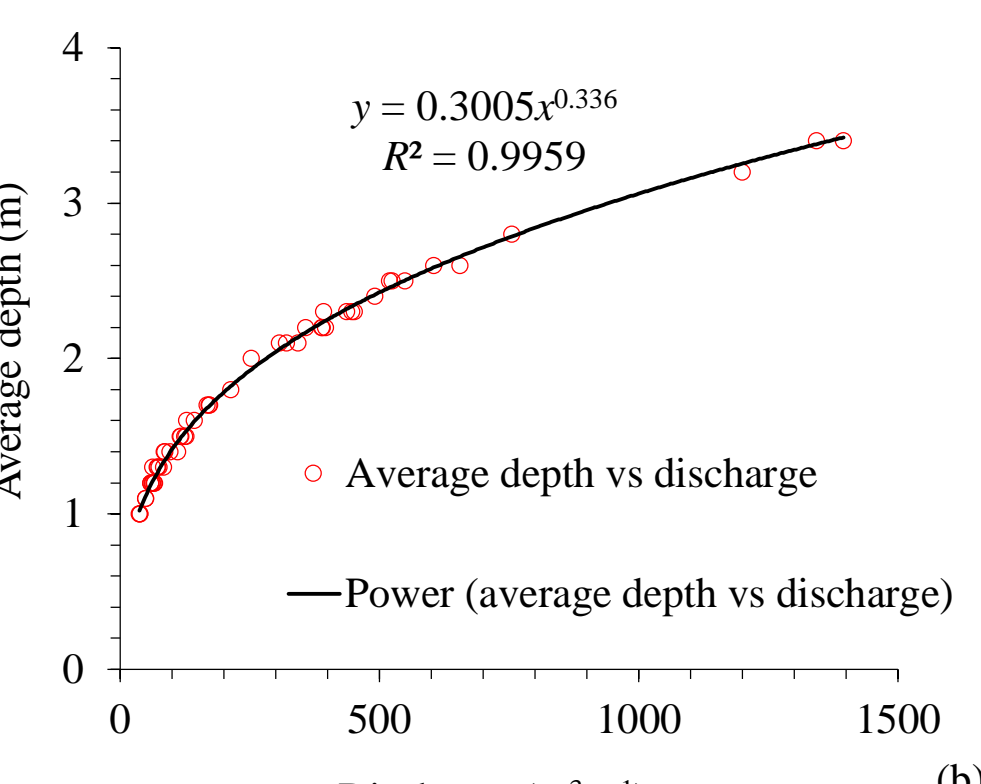


Fig. 6. Scatterplots of effective width (a) and water surface inundation area (b) derived from Landsat images versus river discharge measured at Tanggya gauging station (1999–2018).

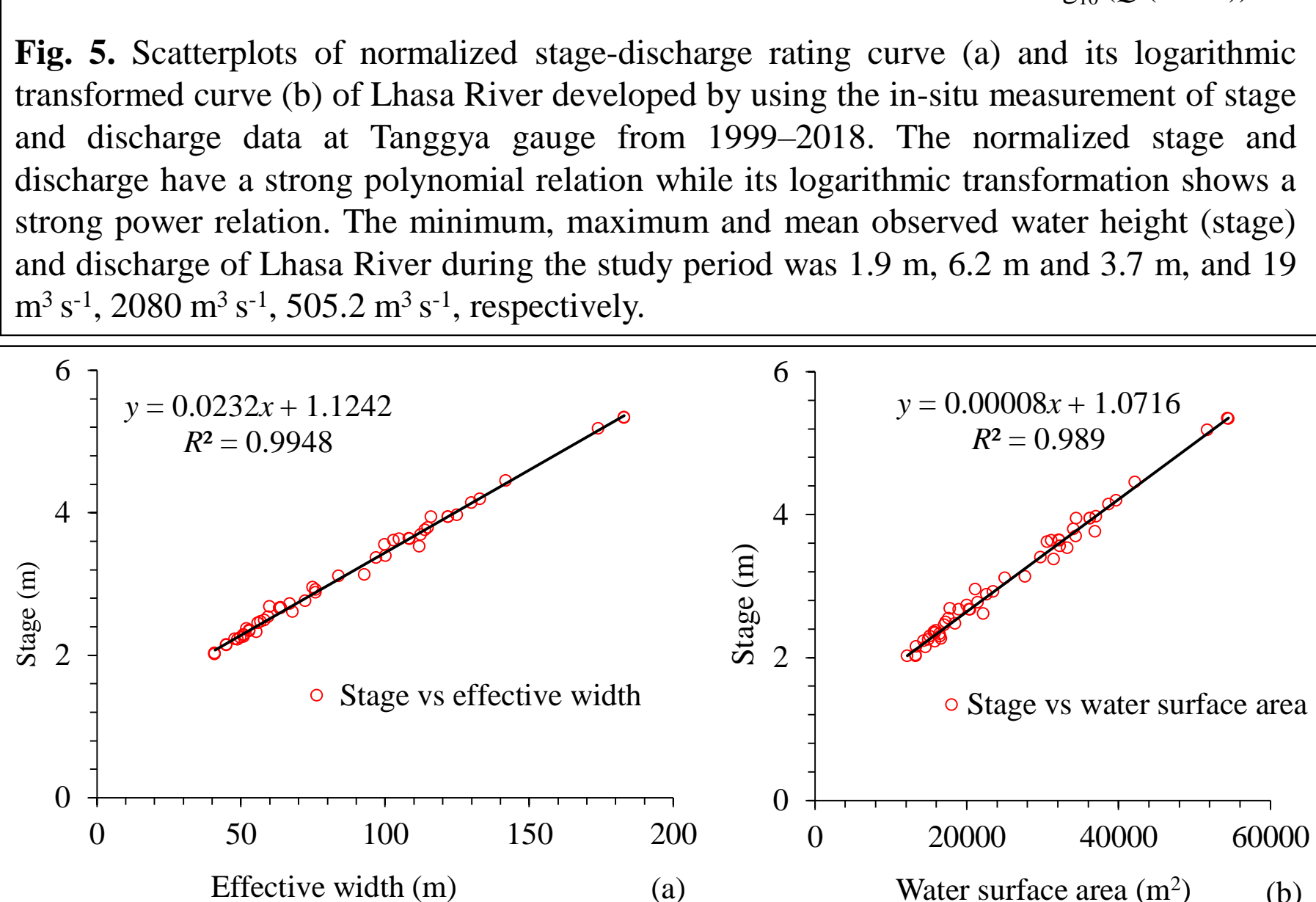


Fig. 7. Scatterplots of stage-water surface inundation area (a) and stage-effective width (b) at Tanggya gauging station (1999–2018). The effective width and water surface inundation area were derived from Landsat image showing a strong linear relationship with stage.

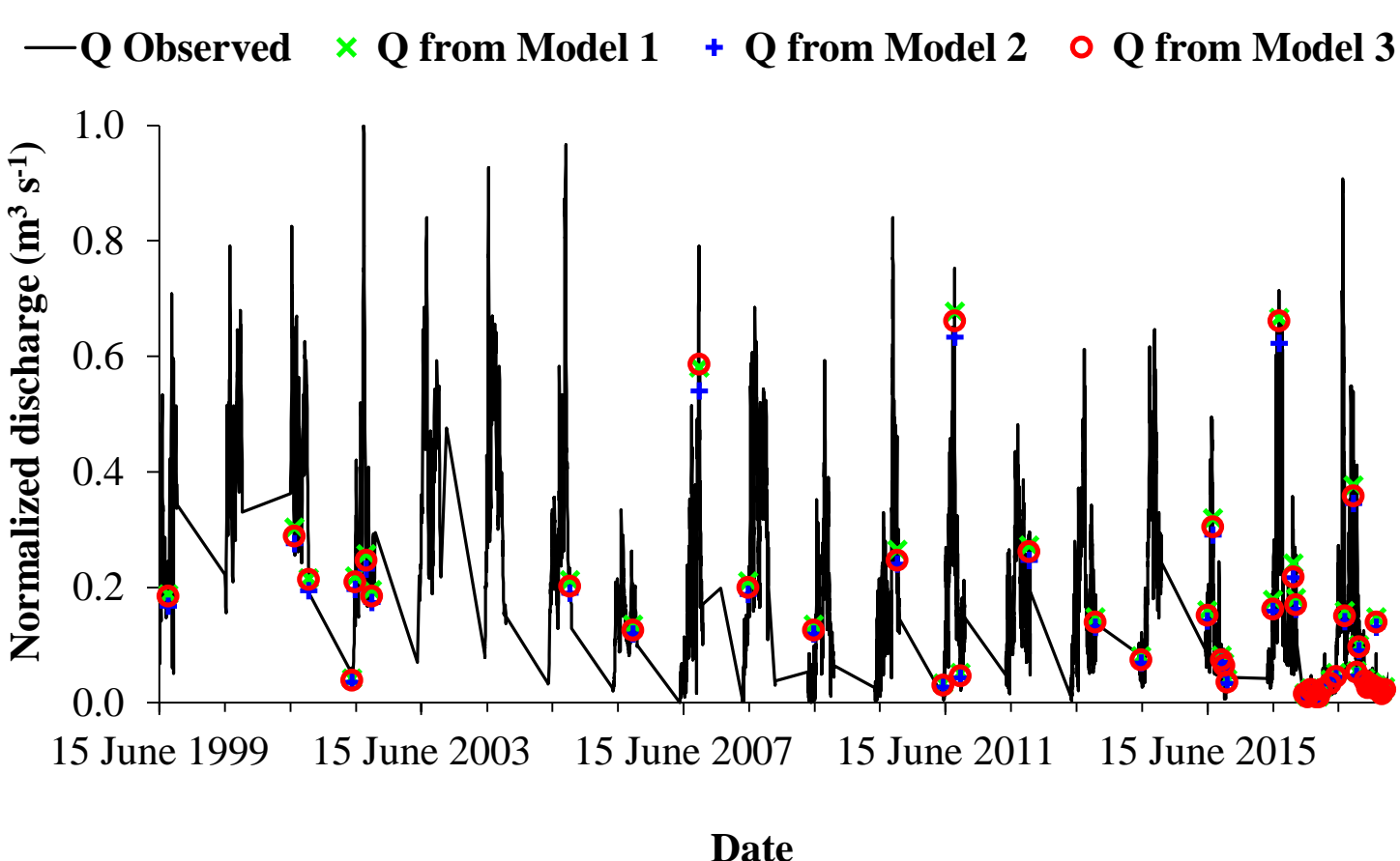


Fig. 8. A comparison plot of time series of discharge estimated by using Model 1, Model 2 and Model 3 with the observed discharge data at Tanggya gauging station (1999–2018). The scatter plots of normalized observed discharge and estimated discharge using Model 1, Model 2 and Model 3 shows a strong linear relationships. The discharge estimated using Model 1, Model 2 and Model 3 with the observed discharge at Tanggya gauging station is very much closer with reasonable accuracy and the two models capture the observed flow pattern very well. In general, estimated discharge values correspond well consistently with the measured ones. But to some extent, generally Model 1 always shows an overestimation of discharge while Model 2 is always underestimating discharge and Model 3 outperforms others.

Table 1. Statistical results of the RMSE, RRMSE, NSE, MBE, and RE for Model 1, Model 2 and Model 3 by using the whole data considered during the study period 1999–2018.

Model	Model performance evaluation methods				
	RMSE ($\text{m}^3 \text{ s}^{-1}$)	RRMSE (%)	NSE	MBE ($\text{m}^3 \text{ s}^{-1}$)	RE (%)
Model 1	20.2	6.84	0.996	15.3	5.2
Model 2	22.3	7.53	0.995	-15.0	-5.1
Model 3	11.4	3.85	0.999	1.1	0.4

Table 2. The performance evaluation results of the RMSE, RRMSE, NSE, MBE, RE, and R^2 statistics in the calibration (1999-2014) and validation (2015-2018) period of the models.

Model	Period	Model performance evaluation methods				
		RMSE (m^3/s)	RRMSE (%)	NSE	MBE (m^3/s)	RE (%)
Model 1	Calibration	22.2	5.0	0.996	-22.0	4.9
	Validation	20.4	9.7	0.994	-20.3	9.7
Model 2	Calibration	27.3	6.1	0.993	20.9	-4.7
	Validation	16.4	7.9	0.996	8.4	-4.0
Model 3	Calibration	12.5	2.8	0.999	-1.1	0.2
	Validation	11.1	5.3	0.998	4.0	-1.9

Conclusions

- This study had innovatively estimated daily river discharge with three different models which are more or less similar to the Surface Water and Ocean Topography (SWOT) observation parameters by combining river surface hydraulic variables directly derived from remote sensing datasets with other variables indirectly derived from empirical equations, which greatly contributes to the improvement of river flow measurement information especially over small rivers of Tibetan Plateau. In addition to this, a successful discharge estimation can be achieved by using width-discharge rating curve approach.
- A strong correlation between in-situ discharge and estimated discharge by the three models distinguishing the seasonal pattern of discharge as well as width and depth variations had been witnessed. The performance of all the three models during the calibration and validation periods also shows the same pattern and signal with the measured discharge (with NSE values ≥ 0.993), meaning that all the three models are capable of estimating Lhasa River discharge in a promising and highly reliable manner.
- Additionally, this study also illustrated that using high spatial resolution remote sensing imagery such as Landsat to extract the river width via MNDWI approach performs quite well at Lhasa River and it could be applied for river discharge estimation especially for narrow mountainous region rivers. The proposed models used in this study should be also further investigated and tested in various river channels environments with respect to the upcoming SWOT mission, which will boost space based discharge estimations studies especially in ungauged and poorly gauged regions.

Acknowledgements

This study was financially supported by the Strategic Priority Research Program of Chinese Academy of Sciences (Grant No. XDA20060202 and XDA19070301) and the National Natural Science Foundation of China (Grant No. 91747201, 41571033). The first author wishes to thank the University of Chinese Academy of Sciences for the scholarship and Arba Minch University, Ethiopia for study leave and financial support. We would also like to thank the United States Geological Survey (USGS) for the Landsat data and SRTM DEM data (earthexplorer.usgs.gov/). Lastly, we are pleased to acknowledge the anonymous reviewers and editor's valuable comments and suggestions to improve this manuscript.

References

- Huang, Q., Long, D., Han, Z., Li, X., and Han P. 2019. "Discharge estimation in ungauged basins in the Tibetan Plateau". AGU Fall Meeting, San Francisco, USA, 9-13 December, 2019.
- Sichangi, A., L. Wang, K. Yang, D. Chen, Z. Wang, X. Li, and D. Kuria. 2016. "Estimating Continental River Basin Discharges Using Multiple Remote Sensing Data Sets." *Remote Sensing of Environment* 179: 36–53. doi:10.1016/j.rse.2016.03.019.
- Tarpanelli, A., S. Barbetta, L. Brocca, and T. Moramarco. 2013. "River Discharge Estimation by Using Altimetry Data and Simplified Flood Routing Modeling." *Remote Sensing* 5 (9): 4145. doi:10.3390/rs5094145.
- Tourian, M. J., C. Schwabke, and N. Sneeuw. 2017. "River Discharge Estimation at Daily Resolution from Satellite Altimetry over an Entire river Basin." *Journal of Hydrology* 546: 230–247. doi:10.1016/j.jhydrol.2017.01.009.
- Wang, L., A. W. Sichangi, T. Zeng, X. Li, Z. Hu, and M. Genanu. 2019. "New Methods Designed to Estimate the Daily Discharges of Rivers in the Tibetan Plateau." *Science Bulletin*. doi:10.1016/j.scib.2019.03.015.
- Moody, J., & B. Troutman. 2002. Characterization of the spatial variability of channel morphology. *Earth Surface Processes and Landforms*, 27, 1251–1266. doi: 10.1002/esp.403.